







# Towards detection of brain injury using multimodal non-invasive neuromonitoring in adults undergoing extracorporeal membrane oxygenation

IRFAAN A. DAR,<sup>1,\*</sup> IMAD R. KHAN,<sup>2</sup> ROSS K. MADDOX,<sup>1,3</sup> OLGA SELIOUTSKI,<sup>4</sup> KELLY L. DONOHUE,<sup>2</sup> MARK A. MARINESCU,<sup>5</sup> SUNIL M. PRASAD,<sup>6</sup> NADIM H. QUAZI,<sup>7</sup> JACK S. DONLON,<sup>1</sup> EMILY A. LOOSE,<sup>7</sup> GABRIEL A. RAMIREZ,<sup>1</sup> JINGXUAN REN,<sup>1</sup>  JOSEPH B. MAJESKI,<sup>1</sup> KENNETH ABRAMSON,<sup>8</sup> TURGUT DURDURAN,<sup>9,10</sup>  DAVID R. BUSCH,<sup>11,12</sup>  AND REGINE CHOE<sup>1,13</sup> 

<sup>1</sup>Department of Biomedical Engineering, University of Rochester, Rochester, New York 14620, USA

<sup>2</sup>Department of Neurology, Division of Neurocritical Care, University of Rochester Medical Center, Rochester, New York 14642, USA

<sup>3</sup>Department of Neuroscience, University of Rochester, Rochester, New York 14620, USA

<sup>4</sup>Department of Neurology, Division of Epilepsy, University of Rochester Medical Center, Rochester, New York 14642, USA

<sup>5</sup>Department of Medicine, Division of Cardiology, University of Rochester Medical Center, Rochester, New York 14642, USA

<sup>6</sup>Department of Surgery, Division of Cardiac Surgery, University of Rochester Medical Center, Rochester, New York 14642, USA

<sup>7</sup>Department of Biology, University of Rochester, Rochester, New York 14620, USA

<sup>8</sup>Department of Physics and Astronomy, University of Pennsylvania, Philadelphia, Pennsylvania 19104, USA

<sup>9</sup>ICFO-Institut de Ciències Fotòniques, The Barcelona Institute of Science and Technology, Castelldefels (Barcelona), 08860, Spain

<sup>10</sup>Institució Catalana de Recerca i Estudis Avançats (ICREA), Castelldefels (Barcelona), 08015, Spain

<sup>11</sup>Department of Anesthesiology and Pain Management, University of Texas Southwestern Medical Center, Dallas, Texas 75390, USA

<sup>12</sup>Department of Neurology, University of Texas Southwestern Medical Center, Dallas, Texas 75390, USA

<sup>13</sup>Department of Electrical and Computer Engineering, University of Rochester, Rochester, New York 14620, USA

\*[idar@ur.rochester.edu](mailto:idar@ur.rochester.edu)

**Abstract:** Extracorporeal membrane oxygenation (ECMO) is a form of cardiopulmonary bypass that provides life-saving support to critically ill patients whose illness is progressing despite maximal conventional support. Use in adults is expanding, however neurological injuries are common. Currently, the existing brain imaging tools are a snapshot in time and require high-risk patient transport. Here we assess the feasibility of measuring diffuse correlation spectroscopy, transcranial Doppler ultrasound, electroencephalography, and auditory brainstem responses at the bedside, and developing a cerebral autoregulation metric. We report preliminary results from two patients, demonstrating feasibility and laying the foundation for future studies monitoring neurological health during ECMO.

© 2020 Optical Society of America under the terms of the [OSA Open Access Publishing Agreement](#)

## 1. Introduction

Extracorporeal membrane oxygenation (ECMO) is a form of cardiopulmonary bypass used to prevent death in patients with acute cardiogenic shock and/or respiratory failure. The goal of ECMO is to deliver adequate perfusion: sufficient, but not excessive, blood flow and oxygen delivery to end organs, including the brain [1]. Despite the risk of over or under cerebral perfusion, ECMO protocols are based on systemic, rather than brain-specific metrics, leaving the brain at risk of injury.

Neurological injury is seen in approximately 25% of adult ECMO patients [2–5]. Hemorrhagic (30%) and ischemic (40%) strokes are not uncommon during ECMO, sometimes leading to brain death. Ischemic strokes have been associated with increased morbidity on discharge [6] and hemorrhages are an independent predictor of mortality [7,8]. In addition to increased mortality, cognition is also significantly reduced in both neonatal and adult ECMO patients with any of the above injuries [9,10]. The pathophysiology of neurologic injury in ECMO is poorly understood, but recent literature suggests that prolonged systemic hypoxia alone does not seem to correlate with poorer outcomes [10].

A critical need exists for non-invasive technology to monitor brain physiology at the bedside for ECMO patients in order to better understand cerebral pathophysiology and learn how to prevent brain injury. Currently, no standardized brain monitoring is performed in clinical practice, partly due to limitations and risks of available technologies. For example, computed tomography (CT) or magnetic resonance imaging (MRI) can detect and localize various injuries such as stroke and hemorrhage, but require complex and risky transportation to scanners. In addition to these hazards, CT and MRI are snapshots in time and are inadequate to monitor neurological health during the days to weeks of ECMO. Cerebral oximetry devices using near-infrared spectroscopy to measure regional cerebral oxygen saturation have increasingly been used in the clinical settings [11], however the reliability of these devices is questionable [12,13]. Additionally, these devices measure changes in oxygen saturation and are unable to provide information of cerebral perfusion which is more pertinent to this patient population.

Diffuse correlation spectroscopy (DCS), transcranial Doppler ultrasound (TCD), electroencephalography (EEG), and evoked potentials (EP) are all low-risk, low-cost alternatives that are suitable for bedside monitoring. DCS uses the interaction between light and moving scatterers, red blood cells, in the cortical microvasculature to obtain blood flow index (BFI) as a surrogate of cerebral blood flow (CBF) [14]. DCS has been used in neonatal ECMO studies [15] as well as assessment of autoregulation and brain injury in other patient populations with brain injuries [16–23]. To complement this measure of microvasculature blood flow, TCD is chosen, which measures the cerebral blood flow velocity (CBFV) of deep cerebral arteries. CBFV from TCD and BFI from DCS have shown good correlation [16,18].

On the other hand, EEG measures cortical activity through a series of electrodes attached to the patient's scalp. EEG provides insight on how the neural compartment of the brain is affected during ECMO treatment compared to the vascular compartment. To further evaluate these EEG signals, alpha to delta ratios (ADR) can be calculated from the alpha and delta waves as a measure of the presence of brain injury in patients with changes in ADR corresponding to change in brain metabolic activity [24]. Patients with neurological injuries have also been shown to have a lower ADR value compared to those without injury, providing an additional marker to evaluate brain health during ECMO treatment [25–27]. While EEG only measures cortical electrical activity, using EP measurements such as auditory brainstem responses (ABR) can provide information on subcortical health. ABR uses auditory stimuli and high acquisition rate from EEG to obtain a signal that comprises of multiple waves which correspond to different locations of the auditory pathway [28]. By measuring the latency of these specific peaks in the response signal, injury to specific regions of the auditory pathway such as the brainstem can be

determined [29,30]. Patients that suffered from neurological injuries showed delayed latencies of specific waveforms or no waveform at all in response to auditory stimuli [31–34].

In addition to changes in CBF, cerebral autoregulation (CA) has been used to evaluate patients for neurological health. Cerebral autoregulation is a set of processes that assist in maintaining appropriate oxygen delivery to the brain, which ensures CBF remains constant at varying cerebral perfusion pressures (CPP) [35,36]. Impairments to this system has been used as a marker for poor neurological outcomes [35]. To measure actual CBF and CPP at the bedside, invasive methods are needed. However noninvasive measures of BFI or CBFV compared to changes in mean arterial pressure (MAP) can be used as a surrogate to evaluate CA [37,38]. By correlating BFI to MAP to obtain a metric such as BFIx [15], periods of dysregulation denoted by high correlation values can be characterized during ECMO treatment.

By combining these modalities and CA analysis, bedside evaluation of brain health can be assessed at both the cortical and subcortical level giving a complete picture of patient health. For this study, we examine the feasibility of using these modalities and demonstrate the use of a CA metric in adult patients that are undergoing ECMO.

## 2. Methods

### 2.1. Device description

Figure 1(a) shows the device setup for this study. DCS probes were placed over the left and right forehead. Multiple EEG electrodes were placed on the scalp as well for continuous monitoring. TCD snapshot measurements were taken on the left and right middle cerebral artery (MCA) by placing an ultrasound probe over the temporal window of the zygomatic arch. Auditory stimuli were presented in both ears, and the response was recorded using an EEG system.

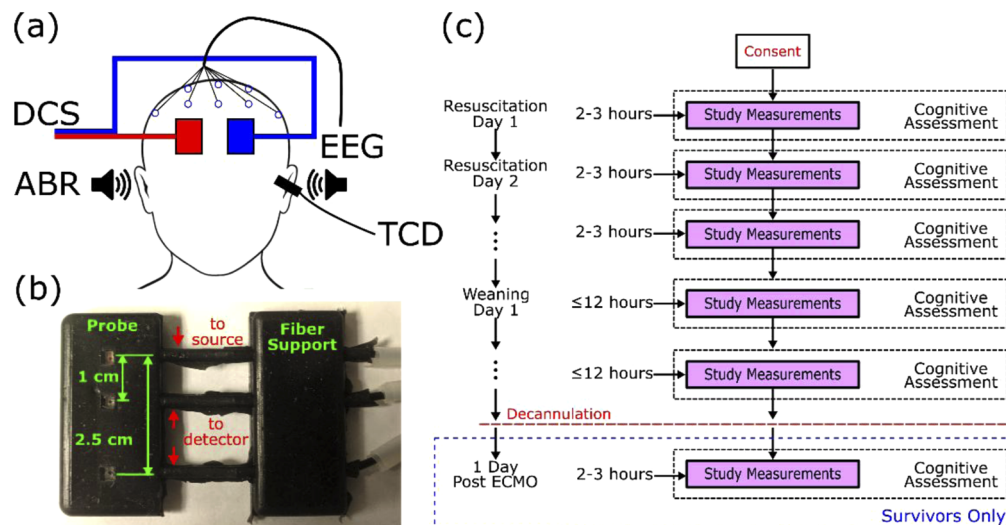


**Fig. 1.** (a) Two optical probes are placed over the left and right hemisphere to acquire cortical CBF from DCS. 16 electrodes are placed on the scalp for quantitative EEG as well as ABR. Earbuds are inserted in both ears for ABR measurements, and an ultrasound probe is placed over the temporal window of the zygomatic arch to measure blood flow from the middle cerebral artery. (b) DCS probe photo. (c) Measurement timeline illustrating phase of ECMO treatment and neuromonitoring recording time for each day. After successful ECMO decannulation, one additional measurement post-ECMO treatment is performed. Bedside cognitive assessments using Glasgow Coma Scale are carried out daily.

### 2.1.1. Diffuse correlation spectroscopy

The DCS instrument is based on the design detailed in previous papers [39,40]. The system in this study consisted of a 785 nm long coherence laser (DL785-120-SO, CrystalLaser, Reno Nevada) with a single 4-channel single photon counting module (SPCM-AQ4C, Excelitas, Waltham, Massachusetts). Each source-detector separation from both probes occupied one channel on the photon counting module. Normalized intensity autocorrelations were calculated using a 4-channel hardware correlator (Flex05OEM, Correlator.com, Bridgewater, New Jersey) every 2 seconds. DCS probes and optical fiber bundles were designed in conjunction with University of Pennsylvania [41] and Fiberoptic Systems (Simi Valley, California). Probes were constructed in-house utilizing fiber bundles custom-built by Fiberoptic Systems, castable elastomer from Smooth-On (Macungie, Pennsylvania), and locally produced molds. Fibers were coupled to the skin utilizing 3 mm prisms (Gurley Precision Optics). The detector fiber bundles (780HP) were positioned 1 cm and 2.5 cm from the source fiber (WF100/110/125). This design of the probes shown in Fig. 1(b) ensured proper contact with the skin over a long period of time and did not obstruct setup of the other modalities [41]. Each probe as shown in Fig. 1(b), included two source detector separations at 1 cm and 2.5 cm to acquire both superficial and cortical blood flow. A 1 × 2 optical switch (S12-M1-N-FC-1-2-S-N, Luminos, Ontario, Canada) connected the laser source to each probe allowing for measurement of both the left and right forehead. The source of each probe was connected to one output of the optical switch, and one short and long separation detector fiber from each probe was connected to a detector channel. Both probes were secured to the head using a 2-sided tape (#1522 and #9917, 3M, Minnesota) and Tegaderm (#16002, 3M, Minnesota) to ensure good contact to the skin. The patient's scalp was checked to ensure the probes were not causing injuries such as skin breakdown during longer recording sessions. Laser power was kept below 27 mW to adhere to American National Standards Institute (ANSI) safety standards [42]. With a 2 second integration time, and laser switching to each probe source, data acquisition for each hemisphere was 0.25 Hz.

### 2.1.2. Transcranial Doppler ultrasound

TCD uses the Doppler shift principle to determine the velocity of red blood cells flowing through a blood vessel. The ultrasound probe is placed over the temporal window of the zygomatic arch to measure the velocity in specific cerebral arteries. A PMD150 TCD device (Spencer Technologies, Redmond, Washington) with a sampling rate of 1 Hz was used. For this study, the ultrasound probe was focused over the MCA with the beam focused at a depth between 40-60 mm. Initially, continuous TCD measurements were to be recorded with a headframe. However due to difficulties encountered in patient comfort and setting up other modalities, TCD snapshot measurements were performed once a day instead. These daily measurements were performed for both the left and right MCA for at least sixty seconds during stable measurements of cerebral blood flow velocity, one MCA at a time. Probe depth, mean, peak, and systolic velocity were recorded.

### 2.1.3. Quantitative electroencephalography

Digital continuous bedside video EEG recording was obtained using either 15 or 19 gold-plated disc electrodes. Electrodes were placed according to the International 10-20 System [43]. For patient 1, electrodes included Fp1, Fp2, F3, F4, C3, C4, P3, P4, T7, T8, A1, A2, Fz, Cz, and Pz. For patient 2, positions P7, P8, O1, and O2 were added to the same 15 electrode positions used for patient 1. EEG data were recorded on a Natus-Xltek system (Natus, Middleton, Wisconsin) in a monopolar montage with all electrodes referenced to FCz in accordance with American Clinical Neurophysiology Society (ACNS) Minimum Technical Requirements [44]. EEG lead maintenance and quality check of the EEG recording was done twice a day. The continuous EEG data were reviewed and interpreted by board-certified electroencephalographer (OS) in

accordance with ACNS recommendations [45]. EEG was recorded for 24 hours each day and was routinely assessed for background organization, presence of epileptiform discharges or seizures. Total duration of the recording was 70+ hours for patient 1 and 160+ hours for patient 2. Quantitative analysis of the EEG was performed by Persyst 13 software (Persyst, Prescott, Arizona). Alpha and delta waves contribution to the EEG recording was determined using a fast fourier transform power analysis. Alpha-Delta ratios (ADRs) were then computed every 15 minutes using the power analysis averaged over a 2-minute window for both left and right hemispheres [24].

#### 2.1.4. Auditory brainstem response

Auditory brainstem responses were recorded using set up similar to that used in previous study [46]. Four EEG electrodes located at Cz (active), FCz (ground), A1 (left ear reference), and A2 (right ear reference) were disconnected from the Neuroworks EEG machine and connected to a V-Amp (Brainvision, Morrisville, North Carolina) EEG system with a sampling rate of 10 kHz. Measurements were recorded using the open source software Labstreaming Layer and custom Python code. Auditory clicks were presented with a 100  $\mu$ s duration with random timing to each ear at a rate of 40 Hz [46] using ER-2 headphones (Etymotic, Elk Grove Village, Illinois) connected to a BabyFace Pro soundcard (RME-Audio, Germany). Stimulus presentation lasted 10 minutes. ABR recordings were performed once each day. After the ABR was acquired, the latency from 0 ms lag to the wave V peak was determined [46].

## 2.2. Clinical protocol

This study was approved by the Institutional Review Board (IRB) at the University of Rochester. Adult patients aged 18 years and older who were admitted to the cardiac intensive care unit (CICU) for ECMO cannulation and treatment at the University of Rochester Medical Center were eligible for this study. The patient's legal representative was approached by a clinician and informed consent was obtained at least 24 hours after initial ECMO cannulation and prior to any study measurements. Patients with prior neurological injuries and facial injuries that would impede study measurements were excluded from the study.

Physiological data was recorded from the Philips Intellivue monitor using Medicollector (medicollector.com) and the ECMO system (Centrimag, Abbott Park, Illinois). Numerical data from the monitor was acquired at 1 Hz and included data such as mean arterial pressure (MAP), heart rate (HR), and respiratory rate (RR), while ECMO speed in rotations/min (rpm) and ECMO flow in liters/min (lpm) were acquired at a rate of 0.2 Hz from the ECMO machine. This data was time-synchronized with all other data acquired.

A schematic of the measurement timeline during the study is shown in Fig. 1(c). The patient's recovery on ECMO is divided into three phases: resuscitation, weaning, and post-ECMO phase. Resuscitation phase is when the ECMO flow and speed are kept constant while the patient recovers. Data was recorded for up to 3 hours during this phase. After a sufficient period of time, if clinical team determines that the patient is ready to be removed from ECMO, the weaning phase begins. During the weaning phase, ECMO speed and flow are gradually reduced to the lowest the patient can handle. Data is recorded for up to 12 hours per day to ensure that changes in the ECMO speed and flow are captured. Finally, if the patient has improved after the weaning phase, ECMO decannulation occurs from the patient and ECMO is discontinued. For post-ECMO phase, a final measurement of up to 2 hours is taken to view the hemodynamics during the patient's native circulation. Measurements were limited to these time periods based on personnel availability to monitor the devices and record clinical events that occurred during the measurement. During each day of measurement, a Glasgow coma scale (GCS) score was conducted at bedside by a neuro-intensivist (IRK) as an evaluation of patient's neural health.

Note that study dates reported in the results section are relative to the first day of measurement and not when initial cannulation of ECMO occurred.

### 2.3. Data analysis: diffuse correlation spectroscopy

All data was analyzed using custom analysis scripts in MATLAB (Mathworks). The normalized intensity autocorrelation curves obtained from the DCS hardware correlator were fitted to a semi-infinite homogeneous solution [14] to extract blood flow index (BFI) using the *fminsearch* function using Nelder-Mead optimization. For the homogeneous solution, a constant absorption coefficient,  $\mu_a$ , of  $0.1 \text{ cm}^{-1}$  and reduced scattering coefficient,  $\mu'_s$ , of  $10 \text{ cm}^{-1}$  were set as described in literature [22,23,47]. For this paper, only the long separation channel of 2.5 cm was analyzed since the DCS signal of this channel contains more cortical contribution than that of the short separation channel. After BFI values were calculated, they were further smoothed with a moving average with a window size of 16 seconds. Figure 2 shows time-synchronized physiological, EEG, ECMO, and TCD data with DCS data. Breaks in BFI data were due to assessing the scalp for skin breakdown every two to three hours. A computer error that required a restart caused the break in physiological data. Autocorrelation curves with a photon count less than 5000 counts per second were discarded due to low signal quality.

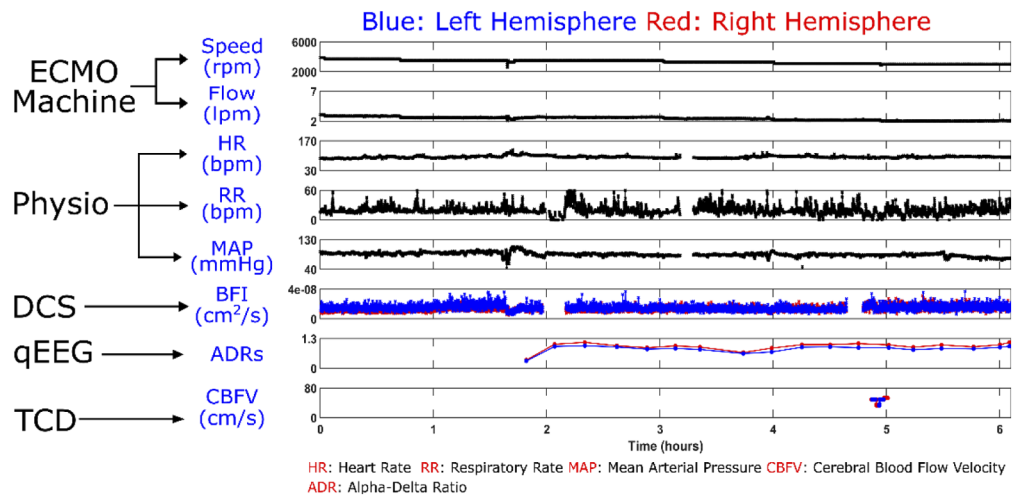


**Fig. 2.** Example of data taken during wean day 1 for patient 1, and the device origin of each signal. Physiological signals are recorded from the bedside Phillips monitor. Breaks in BFI data were due to assessing the scalp for skin breakdown every two hours. The gap in physiological data was due to a computer error requiring a restart.

### 2.4. Data analysis: auditory brainstem response

ABR data was analyzed using Python 3.5 (Anaconda). Data was filtered using a notch filter at 60 Hz harmonics to remove power line noise. Each stimuli was then averaged using a weighting algorithm to obtain the final ABR as defined in previous literature [28]. To further reduce noise, a zero-phase low pass filter was applied to the ABR.

### 2.5. Metric of cerebral autoregulation

To evaluate the degree of cerebral autoregulation, Pearson correlations between MAP and BFI were calculated, defined as BFI<sub>x</sub> in this paper. Both BFI and MAP were resampled to 0.25 Hz using linear interpolation and a moving average window of 10 seconds was used to smooth

MAP data. Based on previous literature on autoregulation moving correlation coefficient, a 5-minute moving window was used to calculate a correlation coefficient [23,48,49]. Correlation coefficients greater than or equal to 0.5 were defined as cerebral dysregulation [50]. Figure 3 shows an example of BFIx calculation. In this figure, a peak in MAP is seen at the 1.4 hour mark as well as a highly fluctuating overall increase starting from 2.8 hour mark. BFI shows similar trend to MAP in these temporal regions, which is reflected in the high BFIx values shown in Fig. 3. To ensure real changes in BFI and MAP are correlated and not the noise in their signal, an exclusion rule was added to the calculation. In the 5-minute moving window, if the MAP range was not greater than 10 mmHg, the data was excluded from the analysis to ensure that BFIx values were not biased due to noise [50,51].

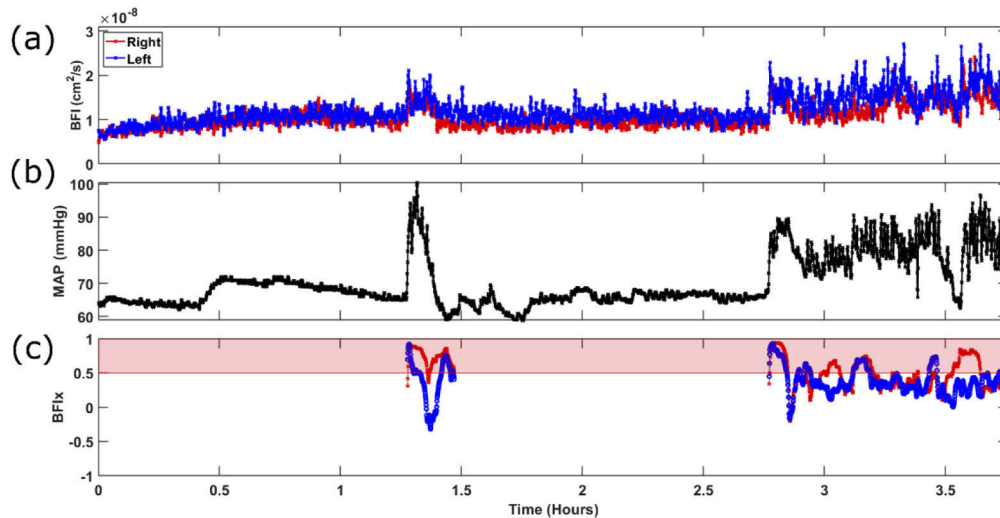


**Fig. 3.** Example of BFIx for patient 2 during weaning day 2. Correlation coefficients between (a) BFI data and (b) MAP data at each time point is shown as (c) BFIx. Red shaded region denotes correlation above 0.5.

To further investigate the patient's autoregulation, Lassen curves are created using BFI and MAP and compared alongside BFIx versus MAP [36]. Lassen curves show the range of cerebral autoregulation where there are minimal changes to CBF over a large range of MAP [52–54]. Dysregulation is shown when CBF increases or decreases alongside MAP. To evaluate these curves for each patient, BFI and MAP signals for each day were combined together and evaluated as a whole. MAP values from the entire recording period for each patient were divided into 1 mmHg increments. BFI and BFIx falling into these MAP groups were averaged and plotted against MAP. Figure 4(a) shows the daily variability of BFI vs MAP. Figure 4(b) shows the Lassen curve generated by averaging over the entire measurement period.

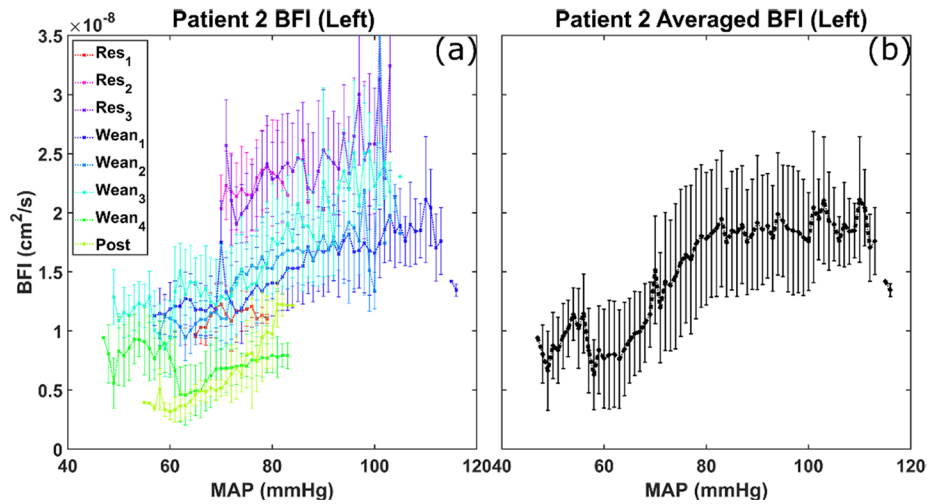


**Fig. 4.** Example of daily BFI values versus average BFI values with respect to changes in the patient's MAP. (a) Average BFI values for each MAP value for each day of patient 2 for the left hemisphere. (b) Daily measurements are combined, and BFI values are averaged over the entire measurement period to obtain an average response of BFI to MAP changes in patient 2 for the left hemisphere. Res#: resuscitation measurement day. Wean#: weaning measurement day. Post: post-ECMO measurement. Error bars for BFI are standard deviation.

### 3. Results

#### 3.1. Patient characteristics

Between December 2019 and February 2020, we recruited a total of 5 patients. In this pilot analysis, we excluded several patients who died during ECMO since we were unable to conclude whether the cause was underlying disease or neurological injury. In this paper, we report two representative patients who survived ECMO, had conclusive neurological outcomes, and had post-ECMO measurements to demonstrate the feasibility of multimodal neuromonitoring and the use of a cerebral autoregulation metric.

Two patients, who were hospitalized for cardiac arrest and required ECMO therapy, were recruited for this study. Patient 1 was a 74-year old female that was admitted for cardiac arrest with no clinical indication of brain injury. Patient 2 was a 53-year-old male admitted for cardiac arrest and was comatose post-arrest. Patient 1 did not receive any CT imaging since she was awake, alert, and following commands during her entire ECMO period. A brain CT scan on patient 2 was performed on day 2 post-arrest (resuscitation day 1) and showed evidence of diffuse hypoxic ischemic encephalopathy (HIE). Both patients were placed on venoarterial ECMO. Study recordings for patient 1 were taken over 4 days, and 8 days for patient 2. Patient 1 co-morbidities included hypertension, hyperlipidemia, coronary artery disease, and congestive heart failure while patient 2 had no significant past medical history except tobacco use.

Both patients were successfully weaned off of ECMO, with Fig. 5 showing ECMO flow, MAP, BFI, and ADR during weaning for both patients. Patient 1 was consented at the start of their weaning off of ECMO, so no measurements during the resuscitation period were performed. Notably, the resuscitation period for patient 1 was only 24 hours due to the patient's rapid recovery. The weaning protocol for patient 1 dropped ECMO speed by 100 rpm starting from 3900 rpm (ECMO starting flow of 3.1 lpm) every 2 hours compared to a drop of 100 rpm every 4 hours for patient 2 starting from 4800 rpm (ECMO starting flow of 4.4 lpm). These drops in ECMO



speed are denoted by the red arrows in Fig. 5 top row plot of ECMO flow. Flow changes not indicated by the red arrows were due to physiological events that may include patient positioning or hyperventilation causing obstructions in the ECMO cannula or changes in the intravascular volume, intra-thoracic pressure or intra-abdominal pressure. Both patients were intubated and received intravenous sedating medications. Patient 1 was neurologically intact, while patient 2 was encephalopathic and agitated during measurement, which led to higher MAP and BFI values. Patient 2 required more circulatory support (higher ECMO flow) than patient 1 (Fig. 5). Total monitoring time for patient 1 was 9.6 hours and 23.4 hours for patient 2. Breaks in data for patient 1 were described for Fig. 2. For patient 2, the break in MAP data was due to an interrupt during data acquisition. For BFI, the break in data was due to checking for skin breakdown. No skin breakdown due to DCS probes was noted for either patient. TCD measurements were recorded by a single operator for patient 1 and the first three days of patient 2. For the remainder of patient 2's monitoring period, a different operator obtained TCD measurements.

### 3.2. Cerebral blood flow analysis

Figure 6 shows average BFI and daily GCS values per day for both patients. Patient 2 exhibited a higher change of BFI over their treatment period compared to patient 1. Increases in BFI were seen from resuscitation day 1 to the final resuscitation day for patient 2, followed by a gradual decrease which led to below day 1 BFI values at post-ECMO. Patient 1 displays smaller relative changes in BFI, but also exhibits a lower blood flow during post-ECMO compared to their first day of measurement. Daily GCS scores for patient 1 did not change, while those for patient 2 increased during the study period, potentially due to the reduction in sedation as well as recovery during the treatment. The dotted line denotes a GCS score of 11, which is the maximum for intubated patients, which both patients were. All BFI data shown in the figures below are from the 2.5 cm source-detector separation. Figure S1 in the supplemental data shows the comparison of short separation and long separation daily BFI values. To evaluate how BFI varies at different ECMO settings for both patients, average BFI and ECMO flow plotted against ECMO speed is shown in Fig. S2 in the supplemental data.

Daily measures of BFI, CBFV, MAP, and ECMO flow are shown in Fig. 7. All values were taken and averaged during the same time period when TCD snapshot measurements occurred. TCD snapshot measurements on average were  $203 \pm 36$  seconds for the right MCA and  $272 \pm 94$  seconds for the left MCA for patient 1. Daily TCD snapshot measurements were  $218 \pm 132$  seconds for the right MCA and  $184 \pm 109$  seconds for the left MCA for patient 2. Relative values of BFI and CBFV to the first day of measurement is also shown in Figs. 7(e) and 7(f).

Similar to the changes in BFI, the CBFV of the right MCA for patient 2 also showed an increase during the resuscitation period followed by a decrease. However, left MCA CBFV measurements were fairly constant across all days. While patient 2 displayed large differences between the trends of BFI and CBFV [Fig. 7(f)], patient 1 showed relatively constant values across all days [Fig. 7(e)]. Variability is seen for patient 2's MAP values [Fig. 7(h)], whereas patient 1 was constant throughout [Fig. 7(g)]. ECMO flow rates were maintained at almost constant level for patient 1 during weaning period [Fig. 7(i)], whereas for patient 2 we see constant flow during the resuscitation period followed by a reduction in flow during the weaning period [Fig. 7(j)].

Averaged percentage of BFIx values greater than 0.5 per hour were calculated each day for both patients and shown in Fig. 8. Results for patient 1 show no percentage of BFIx above the threshold, indicating no correlation between BFI and MAP. Patient 2 in comparison, exhibited a higher percentage of time above the 0.5 threshold which may be due to their underlying HIE.

Figure 9 shows average BFI and BFIx versus MAP for both patient 1 and 2. As the initial analysis, piecewise linear regression fitting under the assumption that autoregulation region can be approximated with a plateau and dysregulation region with a linear line was used to determine the lower MAP starting value of the cerebral autoregulation region on Figs. 9(a) and 9(b). Patient

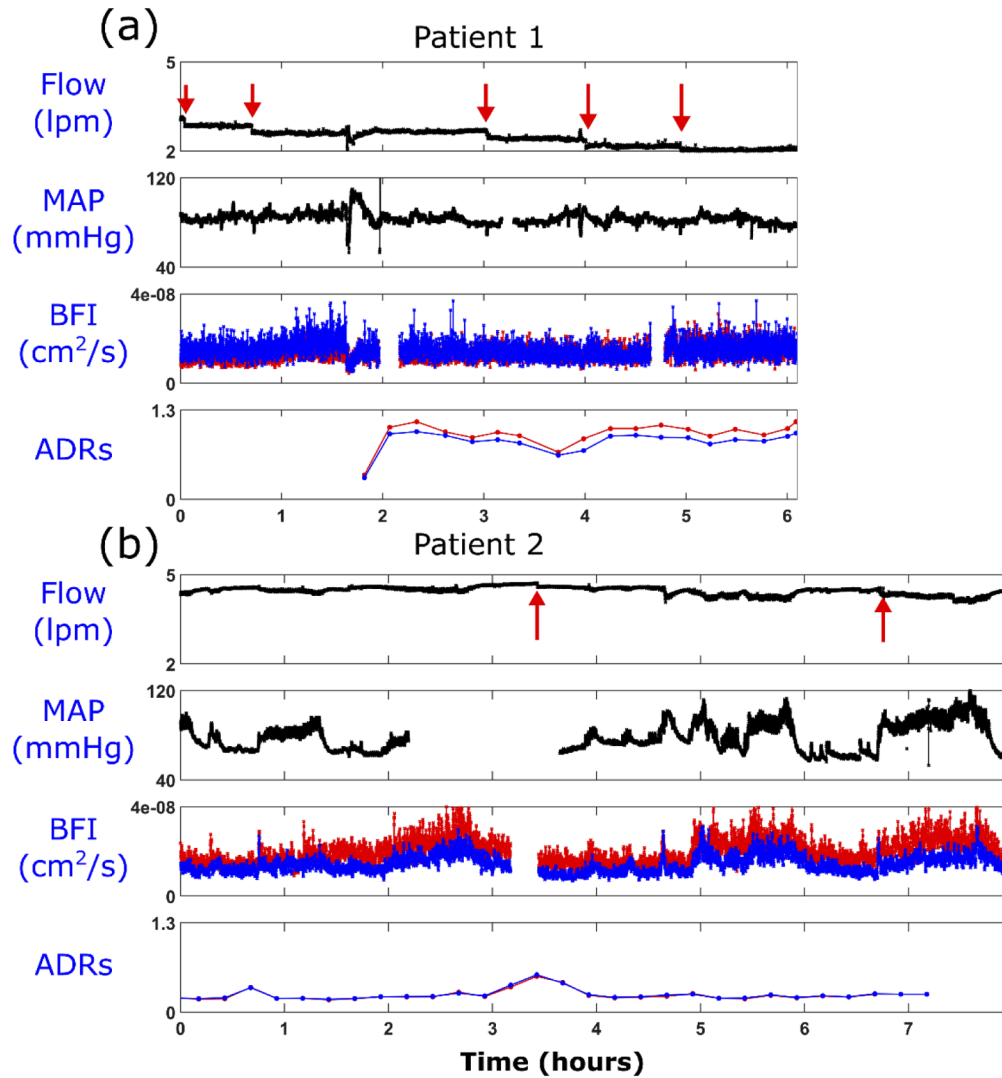


**Fig. 5.** Weaning day measurement for (a) patient 1 with no indication of brain injury and (b) patient 2 who had an indication of hypoxic ischemic encephalopathy from a CT scan obtained on resuscitation day 1. Red arrows indicate when ECMO speed was lowered during the measurement.

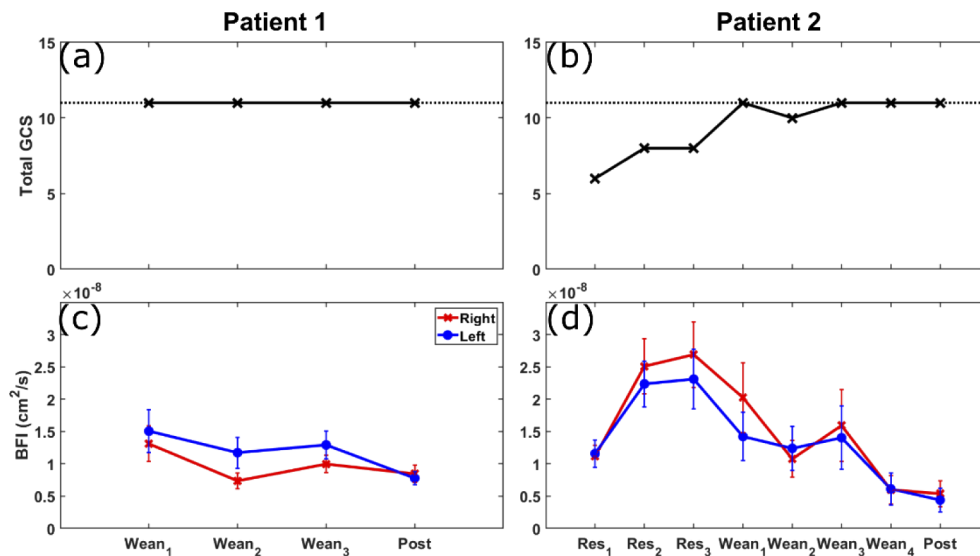


**Fig. 6.** Daily GCS scores for (a) patient 1 and (b) patient 2. Dashed line indicates a GCS score of 11, the maximum for intubated patients. Comparison of averaged BFI per day for (c) patient 1 and (d) patient 2. Monitoring time for patient 1 was 6.1 hours for the first wean day and an average of 1.2 hours for the other days. Monitoring time for patient 2 was 8 hours for wean day 1, 4 hours for wean day 2, and an average of 1.9 hours for the other days. Res#: resuscitation measurement day. Wean#: weaning measurement day. Post: post-ECMO measurement. Error bars for BFI are standard deviation.

1 shows an approximate plateau for MAP values greater than 80 mmHg for both left and right hemispheres. For patient 2, the MAP breakpoint was determined to be 90 mmHg for the right hemisphere and 80 mmHg for the left hemisphere. In Fig. 9(c), patient 1 had no average BFI value above 0.5. However, for patient 2 [Fig. 9(d)], high correlation values are seen for a large range of MAP values.

### 3.3. Electrophysiology analysis

During the measurement period, EEG background in patient 1 demonstrated normal waking with a posterior dominant rhythm of 8.5 Hz and intact sleep organization with normal sleep elements indicative of stage II sleep. Predominant background frequencies included alpha and theta frequency activity with intact reactivity. Frontally predominant intermittent polymorphic diffuse delta slowing was present. The findings were consistent with mild degree of encephalopathy.

Patient 2's EEG background consisted of primarily diffuse disorganized delta activity without evidence of organization of either voltage or frequency gradients. The background lacked variability and reactivity. No sleep elements were noted. The findings were consistent with severe degree of encephalopathy. Neither patient had epileptiform discharges or seizures during monitoring periods.

Average ADRs during measurement periods for patient 1 were 0.82 (right hemisphere) and 0.78 (left hemisphere) and with a range of 0.34-1.13 (right hemisphere) and 0.32-1.11 (left hemisphere). In patient 2, average ADR values were 0.37 (right hemisphere) and 0.37 (left hemisphere) and with a range of 0.16-0.71 (right hemisphere) and 0.15-0.75 (left hemisphere). Daily measures of ADR are shown in Fig. 10. Daily ADR values of patient 1 were constantly higher than that of patient 2 for most days except the last day.

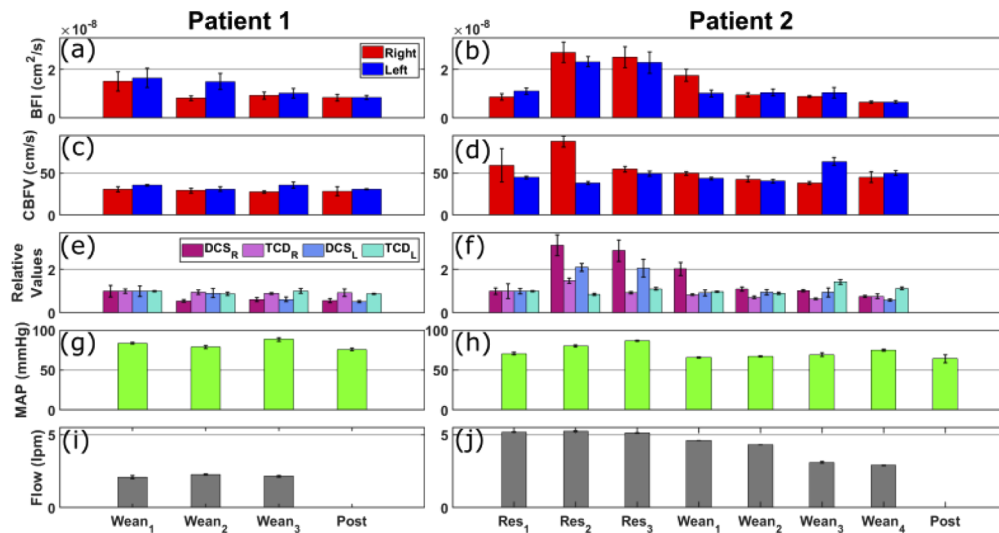


**Fig. 7.** Comparison of changes in BFI, CBFV, MAP, and ECMO flow measurements for (left) patient 1 and (right) patient 2 during TCD measurements. Average TCD measurement time were  $203 \pm 36$  seconds for the right MCA and  $272 \pm 94$  seconds for the left MCA for patient 1 and  $218 \pm 132$  seconds for the right MCA and  $184 \pm 109$  seconds for the left MCA for patient 2. Post ECMO measurements of TCD for patient 2 were discarded due to signal quality, so no BFI is shown for this date. Red indicates right hemisphere and blue indicates left hemisphere measurements. (a,b) Daily BFI values for patient 1 and 2. (c,d) Daily CBFV measurements. (e,f) Relative BFI and CBFV values normalized to day one measurement. (g,h) Daily MAP measurements. (i,j) Daily ECMO flow measurements. Res #: resuscitation measurement day. Wean #: weaning measurement day. Post: post-ECMO measurement.

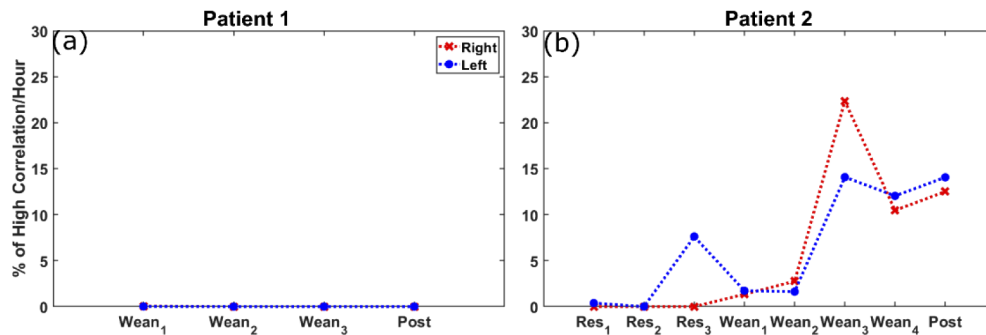


**Fig. 8.** Average % of high correlation values per hour per day for (a) patient 1 and (b) patient 2. Res #: resuscitation measurement day. Wean #: weaning measurement day. Post: post-ECMO measurement.

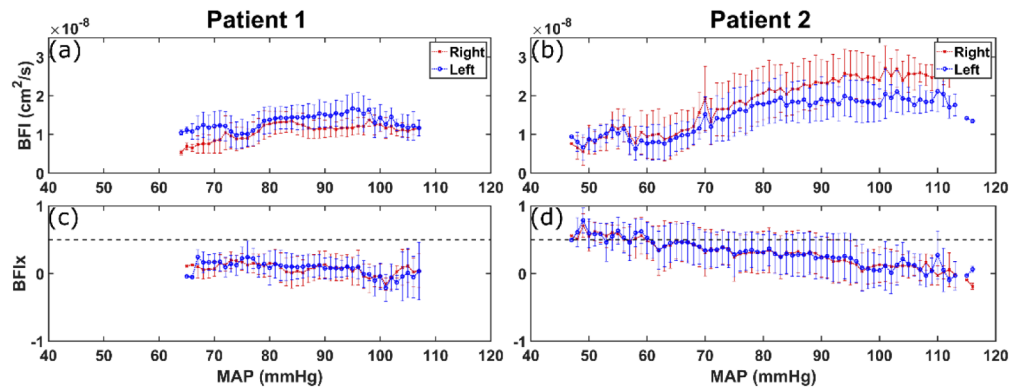


**Fig. 9.** BFI vs MAP for (a) patient 1 and (b) patient 2. BFIx vs MAP for (c) patient 1 and (d) patient 2. Dashed line in bottom graphs indicates 0.5 BFIx threshold. Error bars for BFI and BFIx are standard deviation.

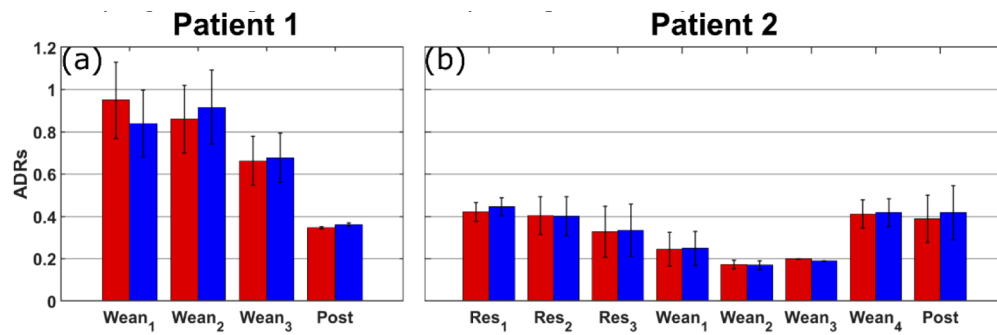


**Fig. 10.** Daily ADR values for (a) patient 1 and (b) patient 2.

ABRs were obtained for patient 1, however for patient 2, the recordings were discarded due to motion artifacts and other electrical interference. Wave V corresponding to neural activity in the inferior colliculus of the brainstem is denoted by the red arrow and clearly seen for patient 1 for every ABR measurement in Fig. 11(a). Calculating the latency to wave V from these waveforms showed a consistent latency across all days for patient 1 [Fig. 11(b)] for both the left and right hemisphere. These are consistent with normal latency range of 6-7 ms for Wave V [46].

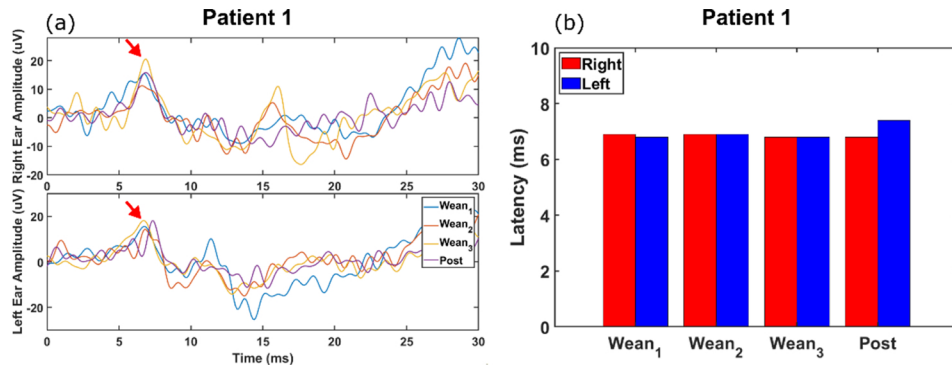


**Fig. 11.** (a) ABR measurements of each day for patient 1. Red arrows indicate the wave V peak for right ear (top) and left ear (bottom). (b) The latency measurement to the wave V peak.

#### 4. Discussion

The goal of this study was to determine the feasibility of using multiple non-invasive modalities for neuromonitoring in patients undergoing ECMO. Currently there is no clinical standard practice in monitoring adult ECMO patients for brain injury. Preliminary results have demonstrated that it was feasible to acquire data on multiple days over the course of the ECMO treatment. This monitoring and cerebral autoregulation analysis provides a foundation for future studies on how ECMO treatment affects neurological outcomes, however further work is needed. To our knowledge this is the first time that DCS was used in adults on ECMO. In addition, this is the first time DCS, TCD, EEG, and ABR have been used together for brain monitoring in adults on ECMO.

##### 4.1. Interpretation of BFIx in preliminary results

As shown in Fig. 8, the percentage of dysregulation per day is higher for patient 2, which may be due to the underlying brain injury. This study used a threshold value of 0.5 as an indication for cerebral dysregulation, however the exact threshold where dysregulation occurs is unknown. Previous literature has shown that the threshold varies between a value of 0.3 to 0.5 when comparing CBFV, BFI, or relative brain oxygen saturation to MAP [35,47,49,50]. Due to this reason, our study chose a threshold value of 0.5 as described in Brady *et al.* [50], but will need to be addressed in future studies as adjustments in this value affect results. While differences were seen in BFIx between these patients, further optimization of the metric is needed. After the optimization, the metric will be tested to determine if brain injuries can be identified during ECMO therapy using more patients. Lassen autoregulation curves in Fig. 9 displays the lower limits of the curve and through linear regression fitting, the MAP breakpoint value was determined for both patients. These breakpoints differ among patients and can provide insight of the optimal MAP range per patient where CBF does not change significantly. Patient 2's breakpoint was at a relatively high MAP value which may be due to autoregulatory impairment (i.e., shrinkage of optimal MAP range), or shift of optimal range due to hypertension. While this shift in their autoregulatory curve may protect the patients from the hypertension, the shift would make them susceptible to hypoperfusion events. At this point, we were not able to obtain BFI values in large enough blood pressure range to estimate the full Lassen curve. In the future, we plan to explore dynamic modulation of ECMO flow setting to address this limitation.

Currently, BFI signals are smoothed using a moving average filter (window size = 16 seconds), however a low pass filter can also be used to reduce high frequency noise. Removing high

frequency fluctuations in BFI through filtering can lead to higher correlations with MAP, but it is not certain whether these fluctuations are pure noise due to BFI fitting or contains crucial hemodynamic information. To address this issue, correlations were discarded if the MAP did not have a range of 10 mmHg to ensure true changes in MAP were correlated, and not noise in the signal [50,51]. Thus, further work is needed to optimize the post processing of BFI to truly evaluate cerebral autoregulation.

#### 4.2. Differences between relative CBFV and BFI

While patient 1 showed agreement between the relative CBFV and BFI changes across days and hemispheres, patient 2 did not. A large difference was seen during the end of the resuscitation period and start of weaning period. Strong correlations are seen between CBFV and BFI in healthy adults and premature infants [17,18,22], which is contrary to what was seen for patient 2 on certain days. The lack of agreement between TCD and DCS values on certain days for patient 2 may be explained by the difference between microvasculature and macrovasculature in terms of how reactivity is influenced. The macrovasculature includes arteries and arterioles, which can be measured by TCD, and reactivity is influenced by the vascular endothelial smooth muscle, systemic blood pressure, and blood gas CO<sub>2</sub>. The microvasculature consists of tissue capillary beds, measurable by DCS [55], and reactivity is influenced by the neuronal activity. Neurovascular coupling is the ability for activated neurons to trigger glial cells to dilate end arterioles just prior to entering capillaries, increasing blood flow into the tissue bed [56]. Neuronal dysfunction from primary or secondary brain injury and sedation can theoretically affect this. Due to the differences in physiologic regulation of CBF at the two locations, it is possible that an insult to microvascular flow may not be recognized at the macrovascular level.

Even though the magnitude of changes in relative CBFV of right hemisphere was less than that of relative BFI, its trend resembled relative BFI: its increase on resuscitation day 2 (Res2) was followed by decrease over time. However, relative CBFV of left hemisphere was relatively stable over time. One possible explanation for this asymmetry between left and right hemispheres for TCD is due to the position of the mixing cloud (i.e., the zone where ECMO-ejected blood flowing retrograde up the aorta meets blood ejected from heart). As the ECMO's flow is weaned, the right side of the brain may be hypo-perfused relative to the left, which still sees flow ejected from the ECMO machine.

#### 4.3. Comparison of ADRs

ADRs in patient 1 were higher on average and demonstrated wider range of variability. In patient 2, ADR values were on average lower and showed lesser range. Low ADR values indicate either decrease in faster (alpha) frequencies, increase in slower (delta) frequencies or both. These findings for patient 2 are commonly occurring in patients with cerebral ischemia [24]. In addition, the overall neurological status of these patients is in keeping with prior reports [25].

#### 4.4. Limitations and future work

There are currently several limitations to our study. By using two probes to measure BFI of the left and right hemisphere, system constraints only allowed us to use one channel to acquire autocorrelation curves at the longer separations. With the lower photon counts at the longer separation, noise is introduced into the autocorrelation curves leading to lower SNR and errors in the BFI fitting. Adding an additional 4-channel detector to capture multiple concurrent autocorrelation curves will allow us to increase the SNR at the longer separations by averaging them together.

Additionally, current results show BFI derived from a homogeneous medium, which is not an accurate representation of the tissue. Implementing a two-layer model to remove the superficial blood flow contamination in the cortical BFI will give a more accurate result of cerebral blood

flow. BFI data from the 2.5 cm separation using the homogeneous solution includes contribution from extracerebral blood flow. By including the 1 cm short separation channel, which primarily measures the superficial layer, and a two-layer model, this extracerebral contribution can be removed [41,57–59].

Furthermore, current optical properties are assumed as constant throughout the study and for each patient, as no frequency-domain or time-domain near-infrared spectroscopy (NIRS) system was used to measure optical properties in real time. In future studies this will need to be addressed by including a frequency or time domain NIRS system.

Regarding TCD measurements, only one attempt to evaluate CBFV of the MCA was done for both hemispheres. In the future, multiple attempts will be carried out to determine sources of error and variability in TCD measurements. To improve reliability in the future, one specific operator would be assigned to measure CBFV of patient as well as carefully comparing different operator's performance in using the TCD device, in case it is not possible to have a single operator per patient. Even though ABR data from only one patient is presented here, our study demonstrates that it is feasible to measure patients in the CICU. Delayed latencies and absence of specific markers of the ABR can identify patients that have subcortical injuries, that the other devices may not be sensitive to. However, motion artifacts as well as electrical interference from other devices corrupted ABR signals as in patient 2's case. Electrical interference can be caused by one of the many clinical equipment used as well as other devices such as cellphones or other wireless devices. An investigation of how these devices affect the EEG system will be performed in the future. Improving the set up and identifying the sources of interference can help improve our acquisition of ABRs. The absence of traditional neuroimaging in some patients is another limitation of the study. With no set clinical protocol of evaluating the patient's health during ECMO due to the high risks involved in transporting patients to imaging, identifying when brain injuries occur is an issue. Currently bedside cognitive assessments are made to evaluate the patient but are not 100% accurate representation of the patient's neural health due to sedation [60–62]. By evaluating the patient when sedation is paused, a more accurate representation of the patient's cognitive health can be assessed. Despite these limitations, this study provides a first step in providing neuromonitoring in a patient population where conventional neuroimaging poses high risk.

## 5. Conclusion

In conclusion, we have demonstrated the feasibility of using DCS, TCD, EEG, and ABR as non-invasive modalities for bedside monitoring on ECMO patients. Differences were seen in cerebral autoregulation, and electrographic activity between patients with or without brain injury. Further data is needed to evaluate when brain injuries occurs and if ECMO treatment has any effect on neurological outcomes.

## Funding

University of Texas Southwestern Medical Center (Margaret Milam McDermott Distinguished Chair in Anesthesiology and Pain Management Fund); University of Rochester (University Research Award).

## Acknowledgments

We would like to thank Melissa J. Polonenko and Madeline S. Cappelloni for their help in ABR setup and processing as well as Ashley R. Proctor for helping with the setup of this study. We also thank the cardiac ICU team at the University of Rochester Medical Center for allowing us to conduct this research. Portions of this work were presented at the OSA Biophotonics meeting in 2020, paper number, Stu2D.4



## Disclosures

The authors declare no conflicts of interest.

See [Supplement 1](#) for supporting content.

## References

1. G. Makdissi and I. W. Wang, "Extra corporeal membrane oxygenation (ECMO) review of a lifesaving technology," *J. Thorac. Dis.* **7**, E166–176 (2015).
2. L. C. Graber, N. Quillinan, E. J. Marrotte, D. L. McDonagh, and K. Bartels, "Neurocognitive outcomes after extracorporeal membrane oxygenation," *Best Pract. Res. Clin. Anaesthesiol.* **29**(2), 125–135 (2015).
3. R. Lorusso, F. Barili, M. D. Mauro, S. Gelsomino, O. Parise, P. T. Rycus, J. Maessen, T. Mueller, R. Muellenbach, J. Belohlavek, G. Peek, A. Combes, B. Frenckner, A. Pesenti, and R. R. Thiagarajan, "In-hospital neurologic complications in adult patients undergoing venoarterial extracorporeal membrane oxygenation: results from the extracorporeal life support organization registry," *Crit. Care Med.* **44**(10), e964–e972 (2016).
4. R. Lorusso, S. Gelsomino, O. Parise, M. Di Mauro, F. Barili, G. Geskes, E. Vizzardi, P. T. Rycus, R. Muellenbach, T. Mueller, A. Pesenti, A. Combes, G. Peek, B. Frenckner, M. Di Nardo, J. Swol, J. Maessen, and R. R. Thiagarajan, "Neurologic injury in adults supported with veno-venous extracorporeal membrane oxygenation for respiratory failure: findings from the Extracorporeal Life Support Organization database," *Crit. Care Med.* **45**(8), 1389–1397 (2017).
5. R. Sutter, K. Tisljar, and S. Marsch, "Acute neurologic complications during extracorporeal membrane oxygenation: a systematic review," *Crit. Care Med.* **46**(9), 1506–1513 (2018).
6. R. F. Gottesman and A. E. Hillis, "Predictors and assessment of cognitive dysfunction resulting from ischaemic stroke," *Lancet Neurol.* **9**(9), 895–905 (2010).
7. S. J. An, T. J. Kim, and B. W. Yoon, "Epidemiology, risk factors, and clinical features of intracerebral hemorrhage: an update," *J. Stroke* **19**(1), 3–10 (2017).
8. M. J. Benko, S. G. Abdulla, J. A. Cuoco, N. Dhiman, B. J. Klein, E. L. Williams, E. A. Marvin, G. A. Howes, B. R. Collier, and M. E. Hamill, "Short- and long-term geriatric mortality after acute traumatic subdural hemorrhage," *World Neurosurg.* **130**, e350–e355 (2019).
9. K. Boyle, R. Felling, A. Yiu, W. Battarjee, J. M. Schwartz, C. Salorio, and M. M. Bembea, "Neurologic outcomes after extracorporeal membrane oxygenation: a systematic review," *Pediatric Critical Care Medicine* **19**(8), 760–766 (2018).
10. V. von Bahr, H. Kalzen, J. Hultman, B. Frenckner, C. Andersson, M. Mosskin, S. Eksborg, and B. Holzgraefe, "Long-term cognitive outcome and brain imaging in adults after extracorporeal membrane oxygenation," *Crit. Care Med.* **46**(5), e351–e358 (2018).
11. J. K. Wong, T. N. Smith, H. T. Pitcher, H. Hirose, and N. C. Cavarocchi, "Cerebral and lower limb near-infrared spectroscopy in adults on extracorporeal membrane oxygenation," *Artif. Organs* **36**, 659–667 (2012).
12. R. A. Kahn and A. Anyanwu, "Near-infrared spectroscopy in vegetables and humans: An observational study," *Eur. J. Anaesthesiol.* **35**(12), 907–910 (2018).
13. A. la Cour, G. Greisen, and S. Hyttel-Sorensen, "In vivo validation of cerebral near-infrared spectroscopy: a review," *Neurophotonics* **5**(4), 040901 (2018).
14. T. Durduran, R. Choe, W. B. Baker, and A. G. Yodh, "Diffuse optics for tissue monitoring and tomography," *Rep. Prog. Phys.* **73**(7), 076701 (2010).
15. D. R. Busch, W. B. Baker, C. D. Mavroudis, T. S. Ko, J. M. Lynch, A. L. McCarthy, G. DuPont-Thibodeau, E. M. Buckley, M. Jacobwitz, T. W. Boorady, K. Mensah-Brown, J. T. Connelly, A. G. Yodh, T. J. Kilbaugh, and D. J. Licht, "Noninvasive optical measurement of microvascular cerebral hemodynamics and autoregulation in the neonatal ECMO patient," *Pediatr. Res.* (2020):
16. D. R. Busch, C. G. Rusin, W. Miller-Hance, K. Kibler, W. B. Baker, J. S. Heinle, C. D. Fraser, A. G. Yodh, D. J. Licht, and K. M. Brady, "Continuous cerebral hemodynamic measurement during deep hypothermic circulatory arrest," *Biomed. Opt. Express* **7**(9), 3461–3470 (2016).
17. W. B. Baker, A. B. Parthasarathy, K. P. Gannon, V. C. Kavuri, D. R. Busch, K. Abramson, L. He, R. C. Mesquita, M. T. Mullen, J. A. Detre, J. H. Greenberg, D. J. Licht, R. Balu, W. A. Kofke, and A. G. Yodh, "Noninvasive optical monitoring of critical closing pressure and arteriole compliance in human subjects," *J. Cereb. Blood Flow Metab.* **37**(8), 2691–2705 (2017).
18. E. M. Buckley, N. M. Cook, T. Durduran, M. N. Kim, C. Zhou, R. Choe, G. Yu, S. Schultz, C. M. Sehgal, D. J. Licht, P. H. Arger, M. E. Putt, H. H. Hurt, and A. G. Yodh, "Cerebral hemodynamics in preterm infants during positional intervention measured with diffuse correlation spectroscopy and transcranial Doppler ultrasound," *Opt. Express* **17**(15), 12571–12581 (2009).
19. D. R. Busch, R. Balu, W. B. Baker, W. Guo, L. He, M. Diop, D. Milej, V. Kavuri, O. Amendolia, K. St Lawrence, A. G. Yodh, and W. A. Kofke, "Detection of brain hypoxia based on noninvasive optical monitoring of cerebral blood flow with diffuse correlation spectroscopy," *Neurocrit. Care* **30**(1), 72–80 (2019).

20. T. Durduran, C. Zhou, B. L. Edlow, G. Yu, R. Choe, M. N. Kim, B. L. Cucchiara, M. E. Putt, Q. Shah, S. E. Kasner, J. H. Greenberg, A. G. Yodh, and J. A. Detre, "Transcranial optical monitoring of cerebrovascular hemodynamics in acute stroke patients," *Opt. Express* **17**(5), 3884–3902 (2009).
21. M. N. Kim, T. Durduran, S. Frangos, B. L. Edlow, E. M. Buckley, H. E. Moss, C. Zhou, G. Yu, R. Choe, E. Maloney-Wilensky, R. L. Wolf, M. S. Grady, J. H. Greenberg, J. M. Levine, A. G. Yodh, J. A. Detre, and W. A. Kofke, "Noninvasive measurement of cerebral blood flow and blood oxygenation using near-infrared and diffuse correlation spectroscopies in critically brain-injured adults," *Neurocrit Care* **12**(2), 173–180 (2010).
22. A. B. Parthasarathy, K. P. Gannon, W. B. Baker, C. G. Favilla, R. Balu, S. E. Kasner, A. G. Yodh, J. A. Detre, and M. T. Mullen, "Dynamic autoregulation of cerebral blood flow measured non-invasively with fast diffuse correlation spectroscopy," *J. Cereb. Blood Flow Metab.* **38**(2), 230–240 (2018).
23. J. Selb, K. C. Wu, J. Sutin, P. I. Lin, P. Farzam, S. Bechek, A. Shenoy, A. B. Patel, D. A. Boas, M. A. Franceschini, and E. S. Rosenthal, "Prolonged monitoring of cerebral blood flow and autoregulation with diffuse correlation spectroscopy in neurocritical care patients," *Neurophotonics* **5**(4), 045005 (2018).
24. B. Foreman and J. Claassen, "Quantitative EEG for the detection of brain ischemia," *Crit. Care* **16**(2), 216 (2012).
25. J. Claassen, L. J. Hirsch, K. T. Kreiter, E. Y. Du, E. S. Connolly, R. G. Emerson, and S. A. Mayer, "Quantitative continuous EEG for detecting delayed cerebral ischemia in patients with poor-grade subarachnoid hemorrhage," *Clin. Neurophysiol.* **115**(12), 2699–2710 (2004).
26. S. P. Finnigan, M. Walsh, S. E. Rose, and J. B. Chalk, "Quantitative EEG indices of sub-acute ischaemic stroke correlate with clinical outcomes," *Clin. Neurophysiol.* **118**(11), 2525–2532 (2007).
27. F. Al-Mufti, K. Amuluru, B. Smith, N. Damodara, M. El-Ghanem, I. P. Singh, N. Dangayach, and C. D. Gandhi, "Emerging markers of early brain injury and delayed cerebral ischemia in aneurysmal subarachnoid hemorrhage," *World Neurosurg.* **107**, 148–159 (2017).
28. R. K. Maddox and A. K. C. Lee, "Auditory brainstem responses to continuous natural speech in human listeners," *eNeuro* **5**(1), ENEURO.0441-17.2018 (2018).
29. S. Benghanem, A. Mazeraud, E. Azabou, V. Chhor, C. R. Shinotsuka, J. Claassen, B. Rohaut, and T. Sharshar, "Brainstem dysfunction in critically ill patients," *Crit Care* **24**(1), 5 (2020).
30. N. J. Washnik, J. Anjum, K. Lundgren, and S. Phillips, "A review of the role of auditory evoked potentials in mild traumatic brain injury assessment," *Trends Hear.* **23**, 233121651984009 (2019).
31. Z. D. Jiang, D. M. Brosi, C. Chen, and A. R. Wilkinson, "Impairment of perinatal hypoxia-ischemia to the preterm brainstem," *J. Neurol. Sci.* **287**(1-2), 172–177 (2009).
32. S. K. Munjal, N. K. Panda, and A. Pathak, "Relationship between severity of traumatic brain injury (TBI) and extent of auditory dysfunction," *Brain Inj.* **24**(3), 525–532 (2010).
33. K. R. Vander Werff and B. Rieger, "Brainstem evoked potential indices of subcortical auditory processing after mild traumatic brain injury," *Ear Hear.* **38**(4), e200–e214 (2017).
34. M. L. James and A. M. Husain, "Brainstem auditory evoked potential monitoring: when is change in wave V significant?" *Neurology* **65**(10), 1551–1555 (2005).
35. M. Czosnyka, K. Brady, M. Reinhard, P. Smielewski, and L. A. Steiner, "Monitoring of cerebrovascular autoregulation: facts, myths, and missing links," *Neurocrit Care* **10**(3), 373–386 (2009).
36. N. A. Lassen, "Cerebral blood flow and oxygen consumption in man," *Physiol. Rev.* **39**(2), 183–238 (1959).
37. E. W. Lang, J. Lagopoulos, J. Griffith, K. Yip, Y. Mudaliar, H. M. Mehdorn, and N. W. Dorsch, "Noninvasive cerebrovascular autoregulation assessment in traumatic brain injury: validation and utility," *J. Neurotrauma* **20**(1), 69–75 (2003).
38. R. B. Panerai, "Cerebral autoregulation: from models to clinical applications," *Cardiovasc. Eng.* **8**(1), 42–59 (2008).
39. A. R. Proctor, G. A. Ramirez, S. Han, Z. Liu, T. M. Bubel, and R. Choe, "Validation of diffuse correlation spectroscopy sensitivity to nicotinamide-induced blood flow elevation in the murine hindlimb using the fluorescent microsphere technique," *J. Biomed. Opt.* **23**(3), 1–9 (2018).
40. J. Ren, S. Han, A. R. Proctor, D. E. Desa, G. A. Ramirez, V. R. D. Ching-Roa, J. B. Majeski, I. A. Dar, N. E. Barber, A. M. Forti, D. S. W. Benoit, and R. Choe, "Longitudinal 3D blood flow distribution provided by diffuse correlation tomography during bone healing in a murine fracture model," *Photochem. Photobiol.* **96**, 380–387 (2020).
41. W. B. Baker, A. B. Parthasarathy, T. S. Ko, D. R. Busch, K. Abramson, S. Y. Tzeng, R. C. Mesquita, T. Durduran, J. H. Greenberg, D. K. Kung, and A. G. Yodh, "Pressure modulation algorithm to separate cerebral hemodynamic signals from extracerebral artifacts," *Neurophotonics* **2**(3), 035004 (2015).
42. D. R. Busch, J. Davis, A. Kogler, R. M. Galler, A. B. Parthasarathy, A. G. Yodh, and T. F. Floyd, "Laser safety in fiber-optic monitoring of spinal cord hemodynamics: a preclinical evaluation," *J. Biomed. Opt.* **23**(6), 1–9 (2018).
43. J. N. Acharya, A. J. Hani, J. Cheek, P. Thirumala, and T. N. Tsuchida, "American Clinical Neurophysiology Society Guideline 2: guidelines for standard electrode position nomenclature," *Neurodiagn J.* **56**(4), 245–252 (2016).
44. S. R. Sinha, L. Sullivan, D. Sabau, D. San-Juan, K. E. Dombrowski, J. J. Halford, A. J. Hani, F. W. Drislane, and M. M. Stecker, "American Clinical Neurophysiology Society Guideline 1: minimum technical requirements for performing clinical electroencephalography," *J. Clin. Neurophysiol.* **33**(4), 303–307 (2016).
45. S. T. Herman, N. S. Abend, T. P. Bleck, K. E. Chapman, F. W. Drislane, R. G. Emerson, E. E. Gerard, C. D. Hahn, A. M. Husain, P. W. Kaplan, S. M. LaRoche, M. R. Nuwer, M. Quigg, J. J. Riviello, S. E. Schmitt, L. A. Simmons, T. N. Tsuchida, and L. J. Hirsch, "Consensus statement on continuous EEG in critically ill adults and children, part II: personnel, technical specifications, and clinical practice," *J. Clin. Neurophysiol.* **32**(2), 96–108 (2015).

46. M. J. Polonenko and R. K. Maddox, "The parallel auditory brainstem response," *Trends Hear.* **23**, 233121651987139 (2019).
47. K. Brady, B. Joshi, C. Zweifel, P. Smielewski, M. Czosnyka, R. B. Easley, and C. W. Hogue Jr., "Real-time continuous monitoring of cerebral blood flow autoregulation using near-infrared spectroscopy in patients undergoing cardiopulmonary bypass," *Stroke* **41**(9), 1951–1956 (2010).
48. M. Ono, Y. Zheng, B. Joshi, J. C. Sigl, and C. W. Hogue, "Validation of a stand-alone near-infrared spectroscopy system for monitoring cerebral autoregulation during cardiac surgery," *Anesth. Analg.* **116**(1), 198–204 (2013).
49. C. Zweifel, C. Dias, P. Smielewski, and M. Czosnyka, "Continuous time-domain monitoring of cerebral autoregulation in neurocritical care," *Med. Eng. Phys.* **36**(5), 638–645 (2014).
50. K. M. Brady, J. K. Lee, K. K. Kibler, P. Smielewski, M. Czosnyka, R. B. Easley, R. C. Koehler, and D. H. Shaffner, "Continuous time-domain analysis of cerebrovascular autoregulation using near-infrared spectroscopy," *Stroke* **38**(10), 2818–2825 (2007).
51. J. M. Lam, J. N. Hsiang, and W. S. Poon, "Monitoring of autoregulation using laser Doppler flowmetry in patients with head injury," *J. Neurosurg.* **86**(3), 438–445 (1997).
52. M. Banaji, I. Tachtsidis, D. Delpy, and S. Baigent, "A physiological model of cerebral blood flow control," *Math. Biosci.* **194**(2), 125–173 (2005).
53. O. B. Paulson, S. Strandgaard, and L. Edvinsson, "Cerebral autoregulation," *Cerebrovasc. Brain Metab. Rev.* **2**, 161–192 (1990).
54. W. I. Rosenblum, "Autoregulatory plateau: does it exist?" *J. Cereb. Blood Flow Metab.* **15**(1), 174–177 (1995).
55. T. Durduran and A. G. Yodh, "Diffuse correlation spectroscopy for non-invasive, micro-vascular cerebral blood flow measurement," *NeuroImage* **85**(Pt 1), 51–63 (2014).
56. A. A. Phillips, F. H. Chan, M. M. Zheng, A. V. Krassioukov, and P. N. Ainslie, "Neurovascular coupling in humans: Physiology, methodological advances and clinical implications," *J. Cereb. Blood Flow Metab.* **36**(4), 647–664 (2016).
57. L. Gagnon, M. Desjardins, J. Jehanne-Lacasse, L. Bherer, and F. Lesage, "Investigation of diffuse correlation spectroscopy in multi-layered media including the human head," *Opt. Express* **16**(20), 15514–15530 (2008).
58. R. B. Saager and A. J. Berger, "Direct characterization and removal of interfering absorption trends in two-layer turbid media," *J. Opt. Soc. Am. A* **22**(9), 1874–1882 (2005).
59. K. Verdecchia, M. Diop, A. Lee, L. B. Morrison, T. Y. Lee, and K. St Lawrence, "Assessment of a multi-layered diffuse correlation spectroscopy method for monitoring cerebral blood flow in adults," *Biomed. Opt. Express* **7**(9), 3659–3674 (2016).
60. M. Fischer, S. Ruegg, A. Czaplinski, M. Strohmeier, A. Lehmann, F. Tschan, P. R. Hunziker, and S. C. Marsch, "Inter-rater reliability of the full outline of UnResponsiveness score and the Glasgow Coma Scale in critically ill patients: a prospective observational study," *Crit. Care* **14**(2), R64 (2010).
61. V. N. Iyer, J. N. Mandrekar, R. D. Danielson, A. Y. Zubkov, J. L. Elmer, and E. F. Wijdicks, "Validity of the FOUR score coma scale in the medical intensive care unit," *Mayo Clin. Proc.* **84**, 694–701 (2009).
62. B. M. Livingston, S. J. Mackenzie, F. N. MacKirdy, and J. C. Howie, "Should the pre-sedation Glasgow Coma Scale value be used when calculating acute physiology and chronic health evaluation scores for sedated patients? Scottish Intensive Care Society Audit Group," *Crit. Care Med.* **28**(2), 389–394 (2000).